Supplementary Information for

Modulation of triplet quantum coherence by guest-induced structural changes in a flexible metal-organic framework

Akio Yamauchi,[1] Saiya Fujiwara,[1] Nobuo Kimizuka,[1,2] Mizue Asada,[3] Motoyasu Fujiwara,[3] Toshikazu Nakamura,[3] Jenny Pirillo,[4] Yuh Hijikata,[5] and Nobuhiro Yanai.*[1,2,6]

*Corresponding author. E-mail: yanai@mail.cstm.kyushu-u.ac.jp

Supplementary Table 1. The summary of EPR measurements. Fit errors are also shown for T_2 and T_1.

Guest	T_2 (μs)		T_1 (μs)		Relative populations ($P_x : P_y : P_z$)	$\|D\|$ (MHz)	$\|E\|$ (MHz)
	High (378 mT)	Low (305 mT)	High (378 mT)	Low (305 mT)			
Empty	0.133 ± 0.002 [a]	0.144 ± 0.002 [a]	1.609 ± 0.087	1.450 ± 0.089	1.00 : 0 : 0	1610	160
H_2O	0.136 ± 0.007	0.156 ± 0.005	4.472 ± 0.179	3.935 ± 0.139	0.95 : 0 : 0.05	1610	160
PrOH	0.615 ± 0.014	0.290 ± 0.041	2.560 ± 0.066	2.133 ± 0.056	1.00 : 0 : 0	1610	160
Py	0.523 ± 0.074	0.564 ± 0.066	4.399 ± 0.133	3.886 ± 0.103	1.00 : 0 : 0	1610	160
FU	1.000 ± 0.107 [a]	1.020 ± 0.091 [a]	4.612 ± 0.118	3.999 ± 0.101	0.95 : 0 : 0.05	1610	160
BQ	1.079 ± 0.121	0.999 ± 0.057	5.660 ± 0.302	5.132 ± 0.290	0.75 : 0.25 : 0	1610	160
THF	0.470 ± 0.024 [a]	0.648 ± 0.012 [a]	3.343 ± 0.081	3.160 ± 0.081	0.95 : 0 : 0.05	1610	160
$CHCl_3$	0.125 ± 0.011	0.101 ± 0.015	1.371 ± 0.037	1.128 ± 0.025	0.95 : 0.05 : 0	1610	160
EtAc	0.096 ± 0.032	0.104 ± 0.022	1.684 ± 0.059	1.548 ± 0.048	0.90 : 0.10 : 0	1610	160
h-Tol	< 0.1	< 0.1	3.009 ± 0.189	2.986 ± 0.151	0.95 : 0 : 0.05	1610	160
EtOH	< 0.1	< 0.1	1.226 ± 0.070	1.047 ± 0.061	0.85 : 0.15 : 0	1610	160
AcNt	< 0.1	< 0.1	1.001 ± 0.093	0.978 ± 0.097	0.80 : 0.20 : 0	1610	160

a) The means and the standard errors of three measurements are shown instead of fit errors.

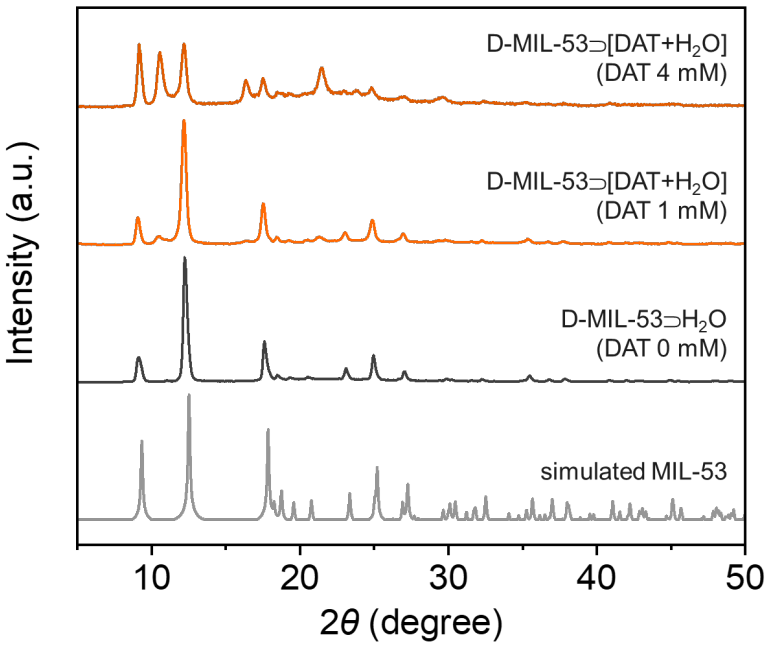

Supplementary Fig. 1. PXRD patterns of D-MIL-53⊃[DAT + H_2O] prepared with DAT in dichloromethane 4 mM (brown) and 1 mM (orange) solution, D-MIL-53⊃H_2O (black), and its simulated pattern (gray).

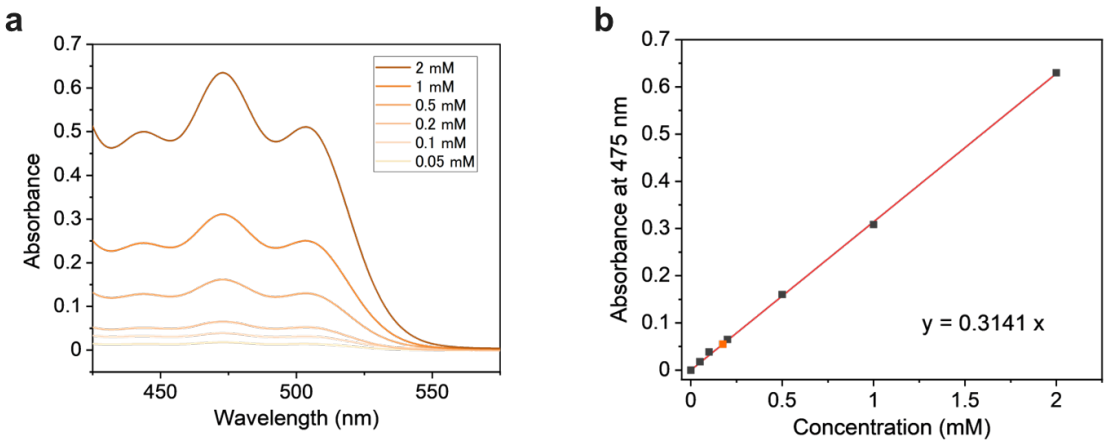

Supplementary Fig. 2. a, UV-vis absorption spectra of a series of DAT standard dichloromethane solutions (0.05, 0.1, 0.2, 0.5, 1, 2 mM). **b**, The calibration line obtained from the absorbance of DAT dichloromethane solutions (0.05 mM, 0.1 mM, 0.2 mM, 0.5 mM, 1 mM and 2 mM) at 475 nm using 1 mm quartz cell. The absorbance at 475 nm was 0.055 when 20.0 mg of D-MIL-53⊃[DAT + H_2O] was digested to 4 mL dichloromethane solution (shown as orange dot). From the calibration curve, the concentration of DAT in the solution was calculated to be 0.175 mM.

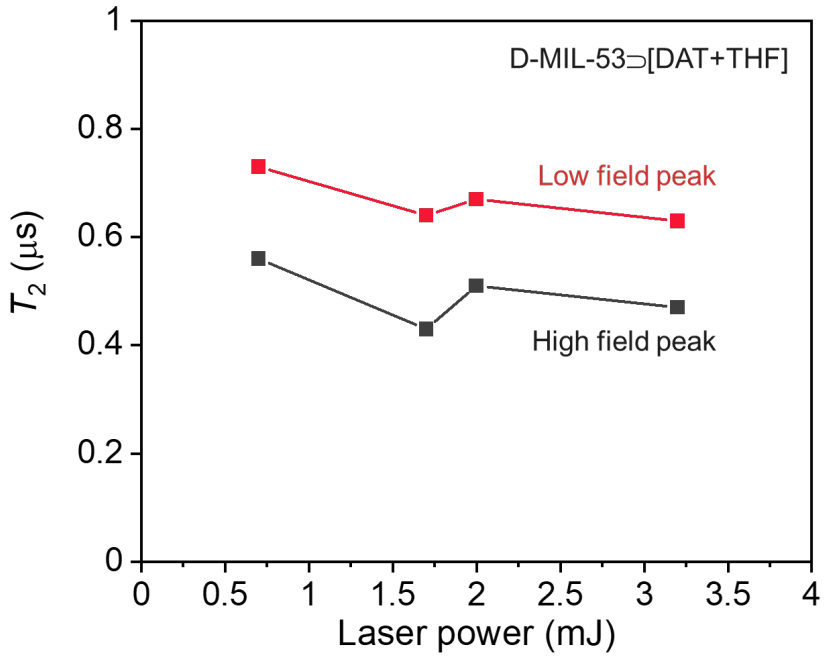

Supplementary Fig. 3. Plot of T_2 against the excitation laser power for the high field peak (black line, 378 mT) and the low field peak (red line, 305 mT) of D-MIL-53⊃[DAT + THF].

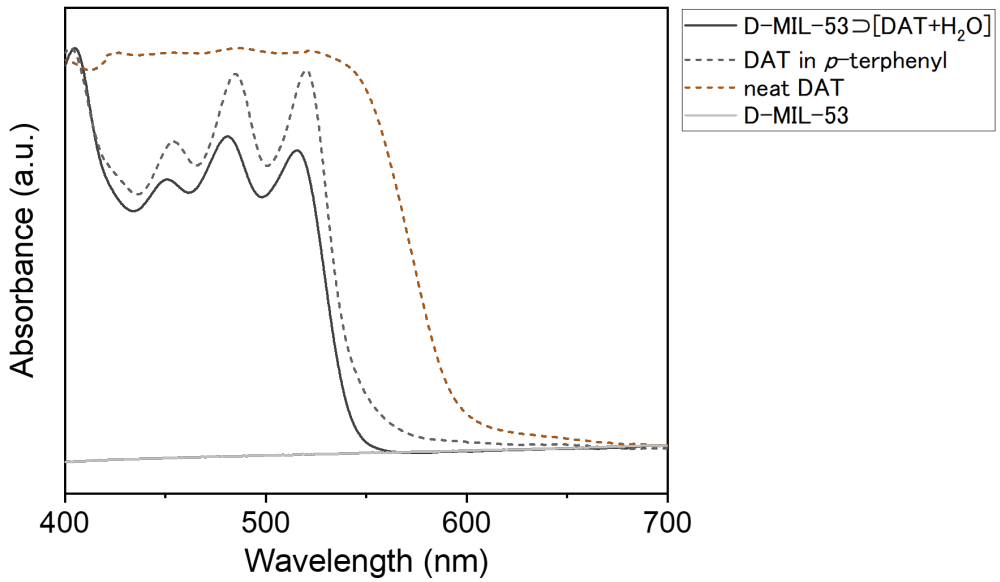

Supplementary Fig. 4. UV-vis absorption spectra of D-MIL-53⊃DAT with H_2O (black line), 0.1 mol% DAT doped in *p*-terphenyl crystal (gray dot line), neat DAT (brown dot line), and D-MIL-53 (gray solid line).

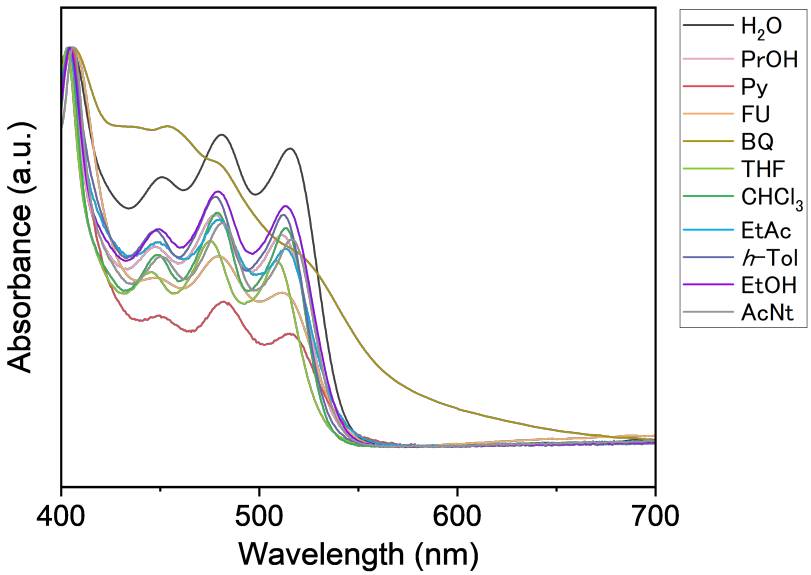

Supplementary Fig. 5. UV-vis absorption spectra of D-MIL-53⊃DAT with H_2O (black), PrOH (pink), Py (red), FU (orange), BQ (yellow), THF (pale green), $CHCl_3$ (green), EtAc (blue), *h*-Tol (dark blue), EtOH (purple), and AcNt (gray). For D-MIL-53⊃[DAT + BQ], the absorption of DAT overlapped with that of BQ.

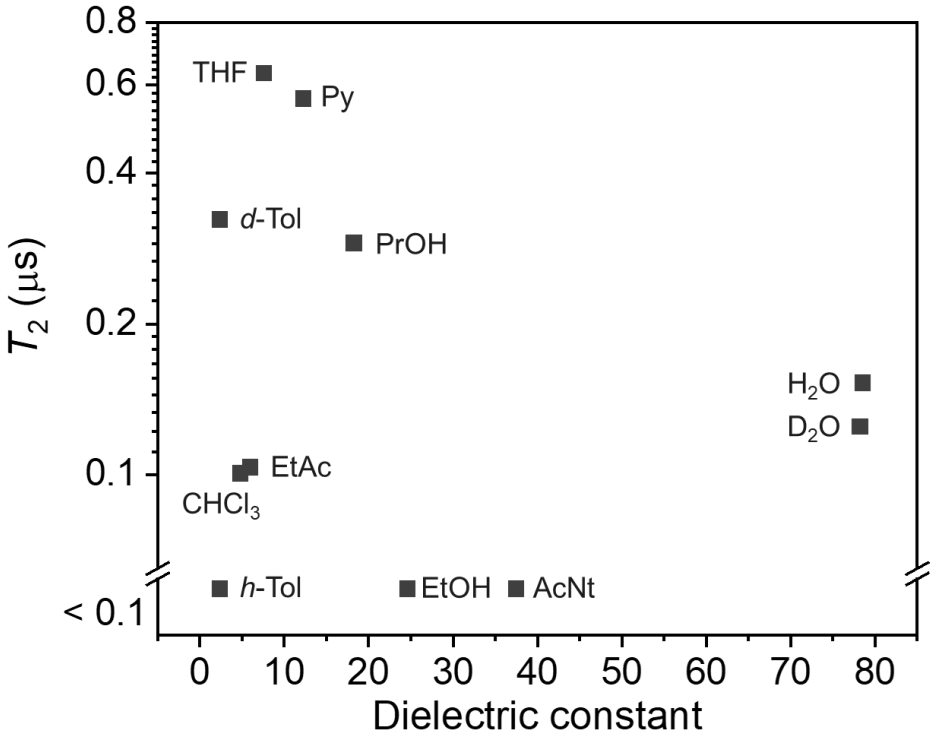

Supplementary Fig. 6. Plot of T_2 of D-MIL-53⊃[DAT + guest] samples against the dielectric constants of the guests. Only liquid guests are plotted.

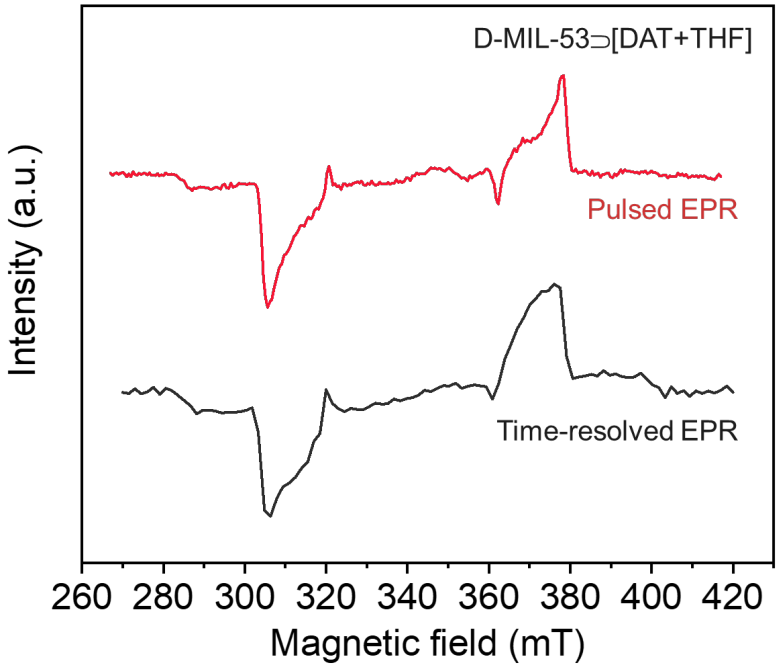

Supplementary Fig. 7. Comparison of the echo-detected field swept spectrum from pulsed EPR (red line) and time-resolved CW-EPR spectrum (black line). The slight changes might be due to the difference in spectral resolution between time-resolved CW-EPR and pulsed EPR, or difference in relaxation times for each peak.

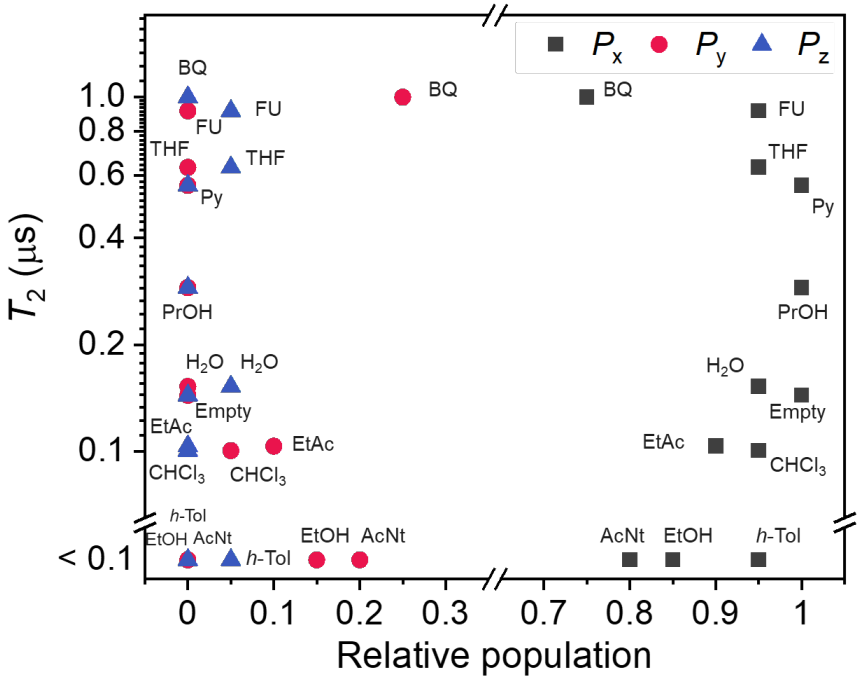

Supplementary Fig. 8. Plot of T_2 against relative populations (P_x : P_y : P_z) of empty (D-MIL-53⊃DAT) and guest-filled (D-MIL-53⊃[DAT + guest]) samples.

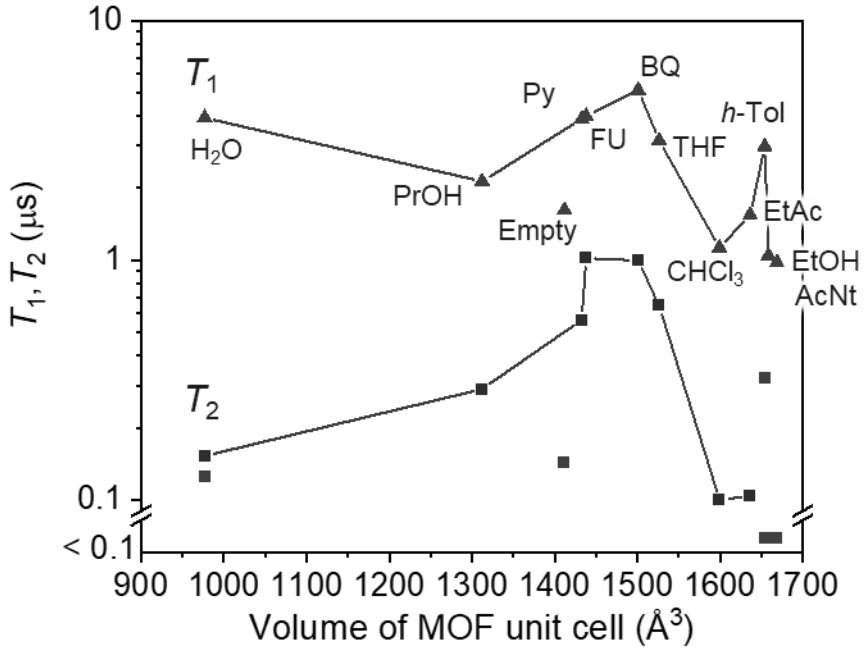

Supplementary Fig. 9. Plot of T_1 (triangle) and T_2 (square) obtained by the single-exponential fitting of time-resolved EPR signal decay and the spin echo decay curves, respectively, against the unit cell volume of MIL-53. Only the values obtained from the low field peaks were shown.

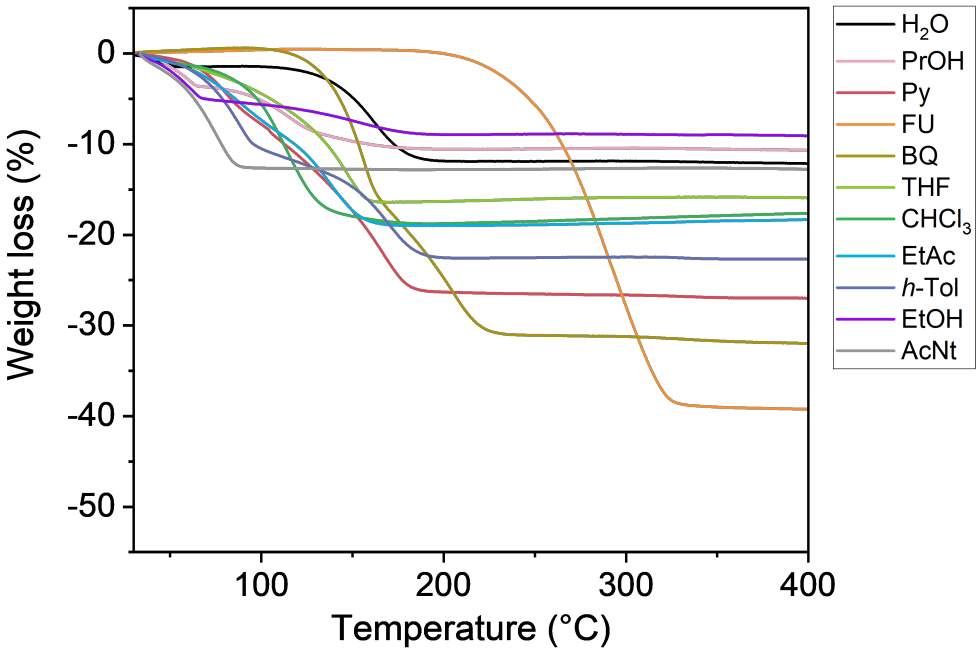

Supplementary Fig. 10. TGA curves of D-MIL-53⊃DAT with H_2O (black), PrOH (pink), Py (red), FU (orange), BQ (yellow), THF (pale green), $CHCl_3$ (green), EtAc (blue), *h*-Tol (dark blue), EtOH (purple), and AcNt (gray). TGA curves were obtained under N_2 atmosphere with a heating rate of 5 °C/min.

Supplementary Table 2. Estimation of guest occupied volume (%) of D-MIL-53⊃[DAT+guest] for each guest.

Guest	Weight loss (%)	m_{guest} (g/mol)	n_{guest} [a]	V_{guest} (Å^3) [a]	V_{MOF} (Å^3) [a]	V_{pore} (Å^3) [a]	Guest occupied volume (%)
H_2O	7.81	18.02	4.022	39.17 [b]	977	638	24.7
PrOH	10.14	60.10	1.607	158.9	1312	973	26.2
Py	26.18	79.10	3.836	151.9 [b]	1433	1094	53.3
FU	39.00	130.08	4.205	160.2	1438	1099	61.3
BQ	31.68	108.10	3.670	190.9 [b]	1501	1162	60.3
THF	16.00	72.11	2.260	203.7 [b]	1526	1187	38.8
$CHCl_3$	18.34	119.38	1.610	140.6 [b]	1599	1261	18.0
EtAc	18.70	88.11	2.234	120.2	1637	1298	20.7
h-Tol	22.48	92.14	2.693	231.2 [b]	1654	1315	47.3
EtOH	8.94	46.07	1.823	119.5 [b]	1659	1320	16.5
AcNt	12.52	41.05	2.983	99.11 [b]	1669	1330	22.2

a) Each value are per 1 unit cell (equivalent to 4 chemical formula or 2 pores).
b) Reported in Ref. 1.

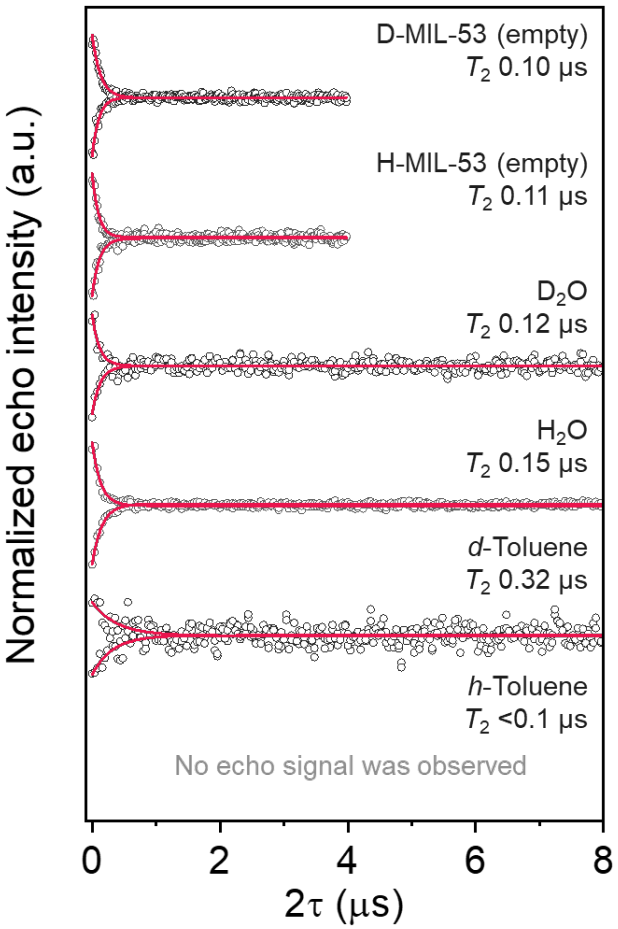

Supplementary Fig. 11. Spin echo decay curves after pulsed photoexcitation at 532 nm for D-MIL-53⊃DAT, H-MIL-53⊃DAT, D-MIL-53⊃[DAT + D_2O], D-MIL-53⊃[DAT + H_2O], D-MIL-53⊃[DAT + *d*-Tol], and D-MIL-53⊃[DAT + *h*-Tol] (from top to bottom) at room temperature. Decay curves of each sample at the magnetic field corresponding to the higher and lower EPR peaks (Fig. 3a) are shown at the top and bottom, respectively. Single-exponential fitting curves for each sample are also shown. Echo signal was not observed for D-MIL-53⊃[DAT + *h*-Tol].

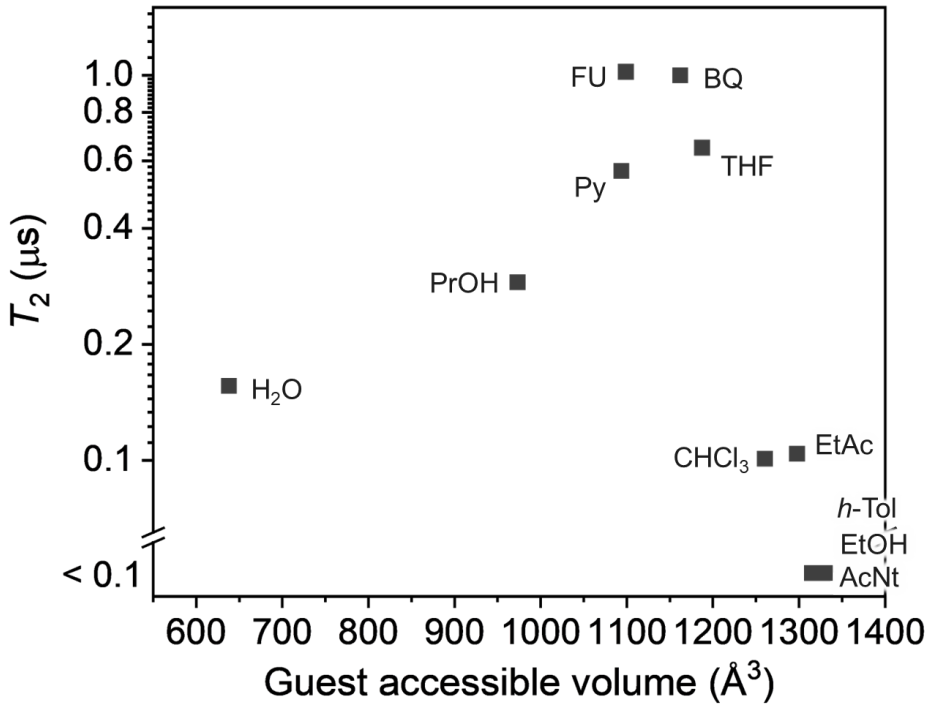

Supplementary Fig. 12. Plot of T_2 against guest accessible pore volume (V_{pore}) of empty (D-MIL-53⊃DAT) and guest-filled (D-MIL-53⊃[DAT + guest]) samples.

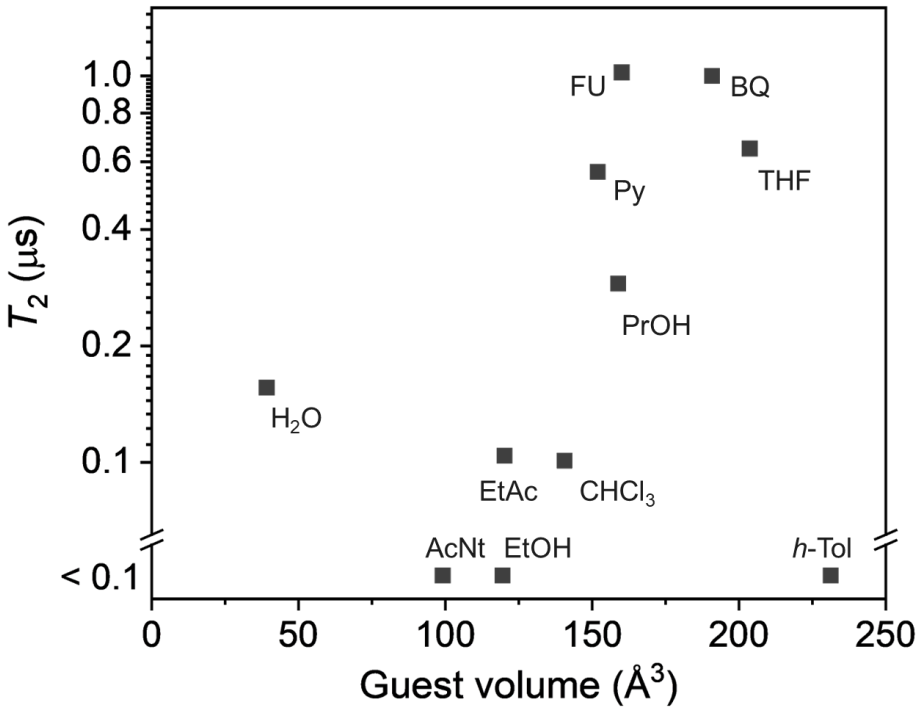

Supplementary Fig. 13. Plot of T_2 against their guest volume (V_{guest}) of empty (D-MIL-53⊃DAT) and guest-filled (D-MIL-53⊃[DAT + guest]) samples.

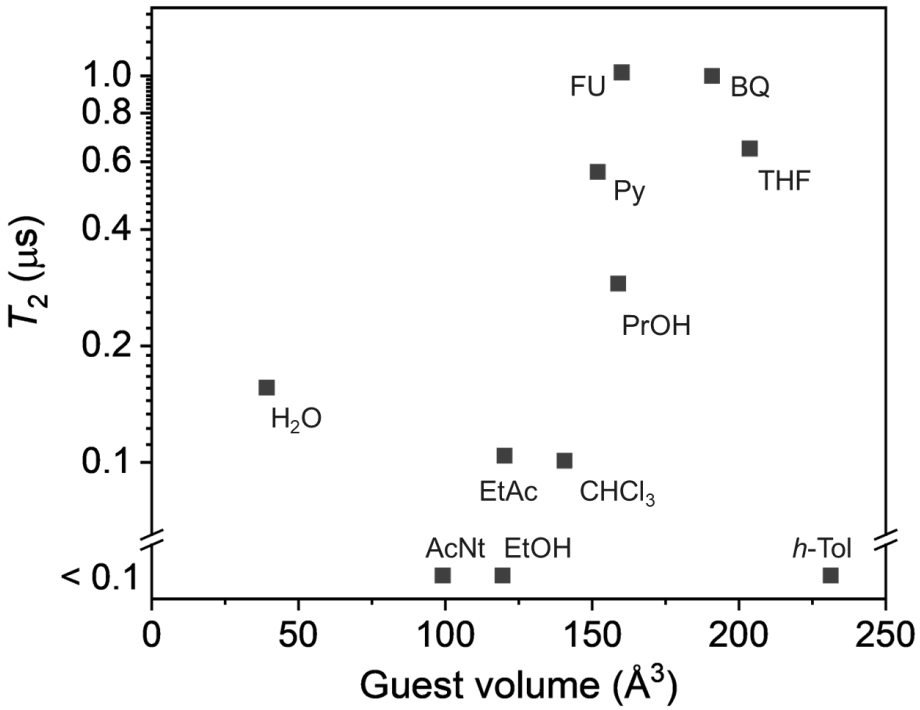

Supplementary Fig. 14. Plot of T_2 against the number of ^{1}H and ^{19}F spins from guest analytes of empty (D-MIL-53⊃DAT) and guest-filled (D-MIL-53⊃[DAT + guest]) samples in a unit cell.

Supplementary Discussion

The relationship between T_2 and each relaxation factors is written as follows:[2]

$$\frac{1}{T_2} = \frac{1}{2T_1} + \frac{1}{T_{ee}} + \frac{1}{T_{en}} \quad \text{(S1)}$$

where T_{ee} and T_{en} were relaxation from dipolar interaction between electron spins and from hyperfine coupling between electron spin and surrounding nuclear spins, respectively. Since the T_1 of our systems were around one magnitude longer than T_2, the spin–lattice relaxation and spin-phonon coupling would not have major role in relaxation. Indeed, for D-MIL-53⊃DAT (denoted as empty), T_2 and T_1 were 0.144 μs and 1.450 μs, respectively. Thus, the value of $(1/T_2 - 1/2T_1)$, which reflects the effect of spin-spin coupling, was calculated as 6.60 μs^{-1} (Supplementary Table 3). This is significantly different from the value for D-MIL-53⊃[DAT+BQ] of 0.90 μs^{-1} (T_2 = 0.999 μs, T_1 = 5.132 μs). Therefore, the effect of spin–spin coupling terms should be main factor for spin–spin relaxation.

The spin–spin interaction of electron spins contains two types of interactions: (i) intermolecular interaction and (ii) intramolecular interaction. The former one is an interaction between triplets in different DAT molecules. Because of low concentration of DAT in the sample (0.87 wt%), this could be neglected as discussed in main text. The latter one is an interaction between electron spins within a single DAT triplet. Triplet electron spin has the dipolar interaction in the composing two spins, this called as zero-field splitting (ZFS). Since ZFS is anisotropic to magnetic field and be fluctuated by the tumbling motions of DAT, the change in the pore density can affects the relaxation rate by the suppression of the tumbling motions through steric hindrance of guests.

For the third term (hyperfine interaction), there are two types of nuclear spins with large gyromagnetic ratio (^{1}H, ^{19}F) in the system: spins on the guest molecules and OH protons attached to aluminum metals (the MOF ligands were deuterated and can be negligible). We plotted T_2 the number of ^{1}H and ^{19}F spins from guest analytes inside a unit cell (Supplementary Fig. 14). If the nuclear spins of guest molecules are dominant to the relaxation, the T_2 should be shorter with the increase of the number of nuclear spins, but such behavior was not observed. Note that some guests with methyl groups like toluene might be exceptional because methyl protons can have significant effect for relaxation (Supplementary Fig. 11, *h*-toluene vs *d*-toluene). The hyperfine coupling between the OH proton and DAT should also exist. While the hyperfine interaction would not be the dominant factor, the degree of fluctuation of hyperfine interaction can be weakened when the tumbling and translational motions of DAT is suppressed by guests.

Thus, the fluctuations of hyperfine interactions and anisotropic ZFS parameters due on the molecular motion of DAT would mainly contribute to the decoherence process. We concluded that these fluctuations that facilitate the relaxation were suppressed by the guest molecules that fill the pore and restrict the motions of DAT qubit as discussed in the main text.

From Supplementary Fig. 9 and Supplementary Table 3, one may find a positive relationship between T_1 and T_2. This would be due to the spin dipolar interaction, which can affect both T_1 and T_2[3]. Since the ZFS interactions induce these relaxations, the relaxation times can be altered when the molecular motion is suppressed. Therefore, the molecular motion of DAT would affect both T_1 and T_2. Although T_1 and T_2 are correlated in this system probably due to the similar origins, T_1 is much longer than T_2

and contribution of spin–lattice relaxation to spin–spin relaxation is less than 12.8 % (Supplementary Table 3), and T_2 should not be limited by spin–lattice relaxation.

Supplementary Table 3. Relationship between T_2, T_1 and other relaxation factors. The value of $1/T_2 - 1/2T_1$ indicates the contribution of other relaxation processes than spin–lattice relaxation.

Guest	T_2 (μs)[a]	T_1 (μs)[a]	$1/T_2$ (μs^{-1})	$1/2T_1$ (μs^{-1})	$1/T_2 - 1/2T_1$ (μs^{-1})	Contribution of spin–lattice relaxation in T_2 (%)[b]
Empty	0.144	1.450	6.94	0.345	6.60	4.97
H_2O	0.156	3.935	6.41	0.127	6.28	1.98
PrOH	0.290	2.133	3.45	0.234	3.21	6.80
Py	0.564	3.886	1.77	0.129	1.64	7.26
FU	1.020	3.999	0.98	0.125	0.86	12.8
BQ	0.999	5.132	1.00	0.097	0.90	9.73
THF	0.648	3.160	1.54	0.158	1.38	10.3
$CHCl_3$	0.101	1.128	9.90	0.443	9.46	4.48
EtAc	0.104	1.548	9.62	0.323	9.29	3.36
h-Tol	< 0.1	2.986	> 10	0.167	> 9.83	< 1.67
EtOH	< 0.1	1.047	> 10	0.478	> 9.52	< 4.78
AcNt	< 0.1	0.978	> 10	0.511	> 9.49	< 5.11

a: the values in lower magnetic field were used.

b: calculated from $(1/2T_1) / (1/T_2) = T_2 / 2T_1$.

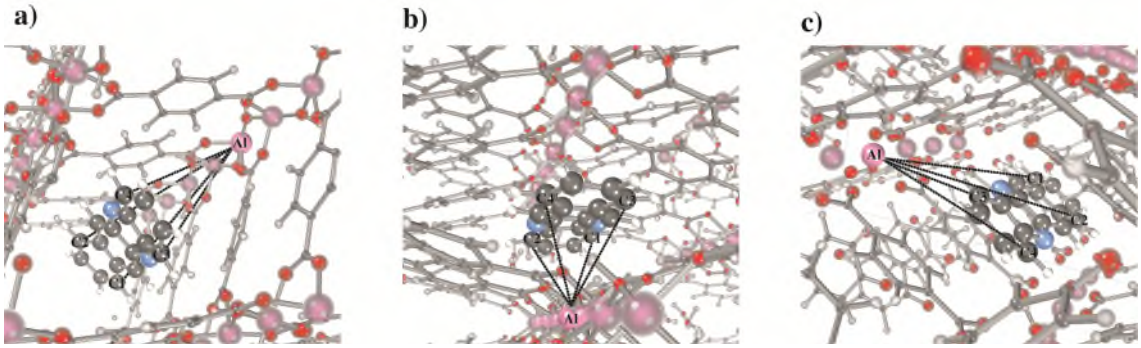

Supplementary Fig. 15. Locations of the aluminum atom and the selected four carbon atoms of the DAT molecule to define the four specific distances in the empty (a), H_2O-solvated (b) and BQ-solvated (c) phases. The dashed four lines in each phase represent these distances which were chosen to analyze the mobility of DAT molecule inside the MIL-53 pore during the MD simulations.

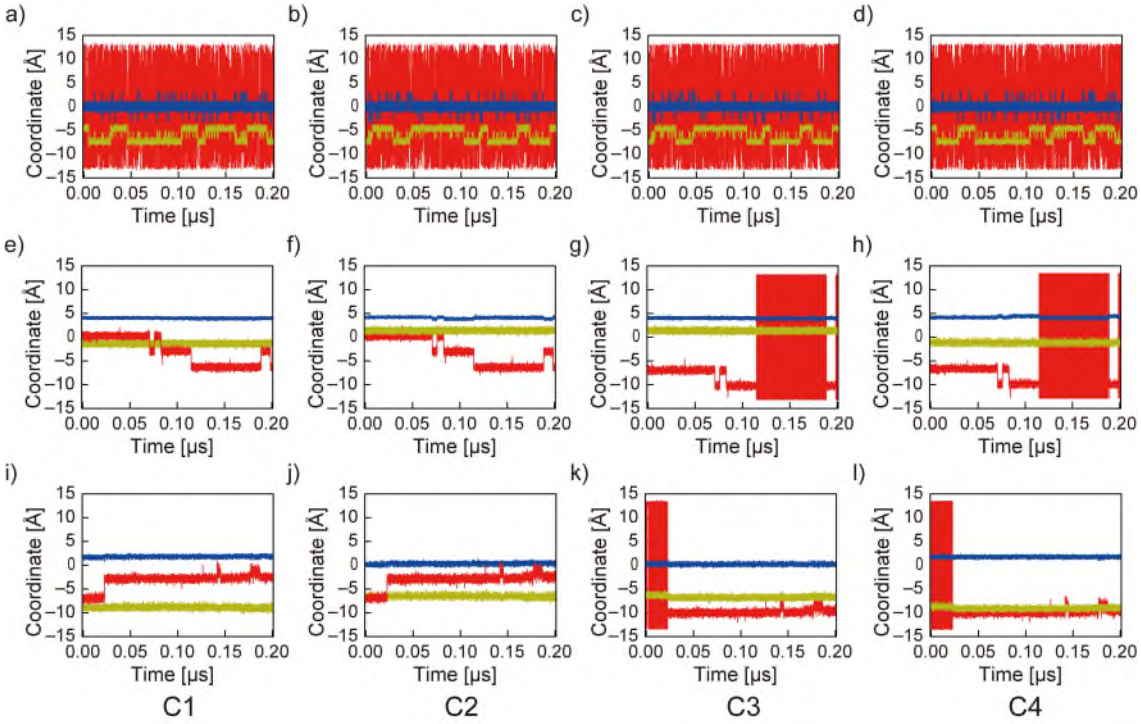

Supplementary Fig. 16. The plots of cartesian coordinates, x (blue), y (ocher) and z (red) of the four carbon atoms shown in Supplementary Fig. 15 during the MD simulation. The origin of the cartesian coordinates is Al atom shown in Supplementary Fig. 15. The plots of empty (a–d), H_2O-solvated (e–h) and BQ-solvated (i–l) phases are shown. Note: The frequent change of the sing for z coordinate, which corresponds to the one-dimensional pore direction of MIL-53, is attributed to the crossing of the boundary of the model cell under the periodic boundary condition.

Supplementary Table 4. Standard deviations of change of the distances between Al atom in the MIL-53 and the four C atoms in DAT shown in Supplementary Fig. 15 for three investigated empty, H_2O-solvated, and BQ-solvated phases.

Phase	Al–C1 / Å	Al–C2 / Å	Al–C3 / Å	Al–C4 / Å
Desolvated	2.8	2.8	2.9	2.8
H_2O-solvated	1.5	1.5	2.3	2.3
BQ-solvated	0.7	0.8	0.9	0.7

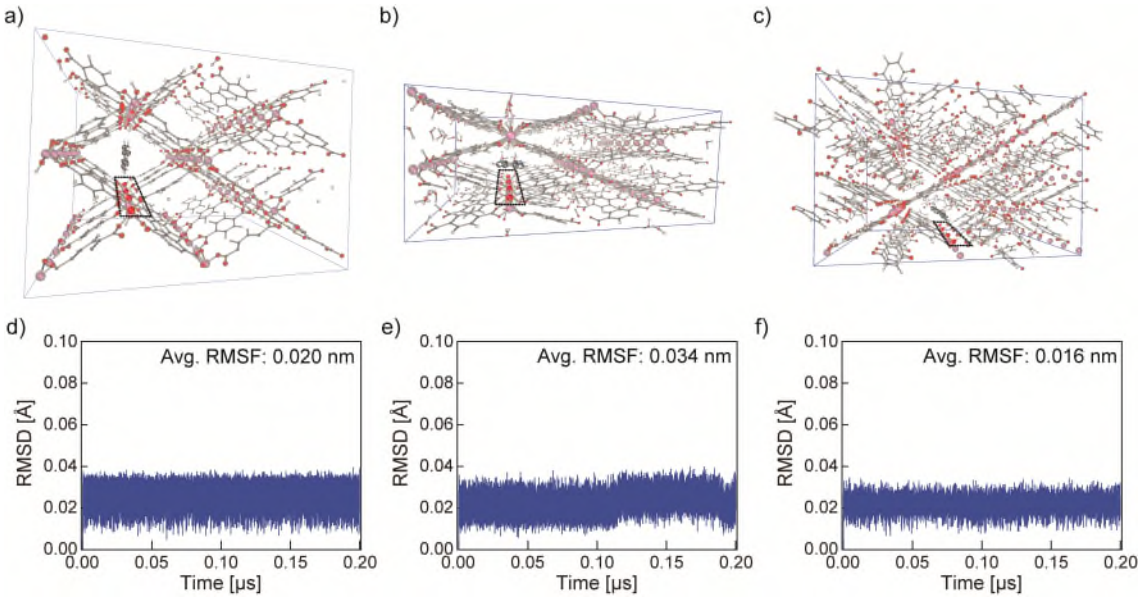

Supplementary Fig. 17. The four μ-OH groups that are close to the DAT molecule shown in the black dashed line in the empty (a), H_2O-solvated (b) and BQ-solvated (c) phases and used to evaluate the root mean square deviation (RMSD) and root mean square fluctuation (RMSF), which are shown in (d), (e), and (f), respectively.

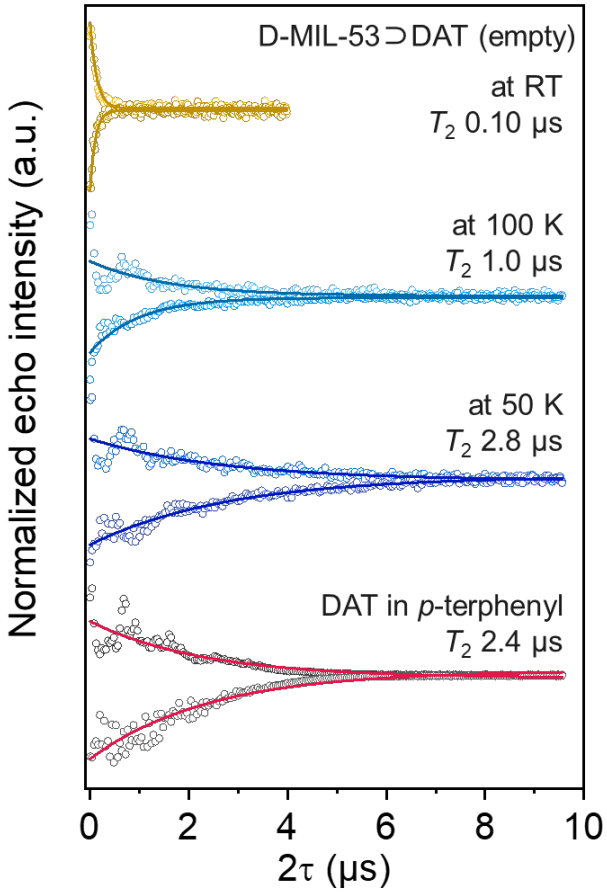

Supplementary Fig. 18. Spin echo decay curves after pulsed photoexcitation at 532 nm for the empty sample (D-MIL-53⊃DAT) at room temperature, 100 K, and 50 K (top to bottom), and for DAT doped in *p*-terphenyl crystal at room temperature. Decay curves of each sample at the magnetic field corresponding to the higher and lower EPR peaks (Fig. 3a) are shown at the top and bottom, respectively.

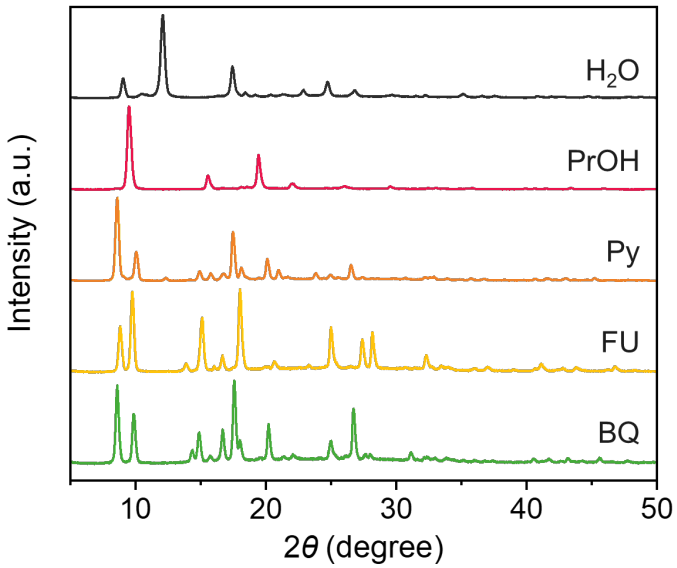

Supplementary Fig. 19 PXRD patterns of D-MIL-53⊃[DAT + H_2O] (black), D-MIL-53⊃[DAT + PrOH] (red), D-MIL-53⊃[DAT + Py] (orange), D-MIL-53⊃[DAT + FU] (yellow), and D-MIL-53⊃[DAT + BQ] (green).

Supplementary Table 5. Steric parameters of the guest molecules: *L*, *h* and *e* are the maximum length, the intermediate length, and the thickness of molecules, respectively. V_{guest} was determined by $L \times h \times e$.

Guest	*L* (Å)	*h* (Å)	*e* (Å)	V_{guest} (Å^3)
PrOH	6.5	5.2	4.7	158.9
FU	6.9	6.7	3.5	160.2
EtAc	6.2	5.7	3.4	120.2

Supplementary Table 6. Unit cell parameters for MIL-53 (Al) with guest molecules.

Guest	a (Å)	a' (Å)	b (Å)	c (Å)	β (°)	V_{MOF} (Å^3)	Crystal system
H_2O[a)]	19.513	18.913	7.612	6.576	104.24	977	monoclinic
PrOH	19.133	18.161	10.844	6.663	108.34	1312	monoclinic
Py	17.547	-	12.181	6.703	-	1433	orthorhombic
FU[b)]	17.984	-	11.749	6.810	-	1438	orthorhombic
BQ	18.642	-	11.916	6.757	-	1501	orthorhombic

a' is the reduced unit cell edge length and $a' = a\cos(\beta-\pi/2)$.
a) Reported in Ref. 4.
b) Reported in Ref. 5.

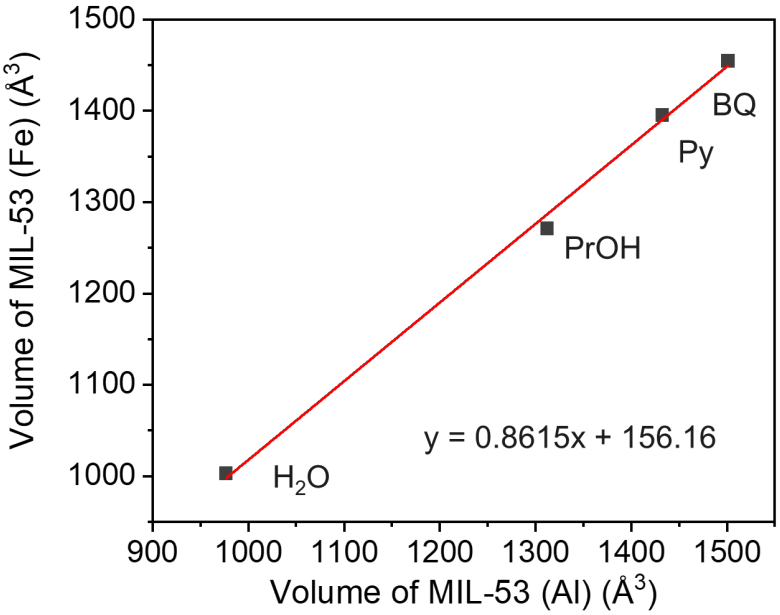

Supplementary Fig. 20. Plot of the volumes of MIL-53 (Fe)⊃guest against those of MIL-53 (Al)⊃guest. The volumes of MIL-53 (Al) with THF, $CHCl_3$, EtAc, *h*-Tol, EtOH and AcNt were estimated from this relationship using reported values of MIL-53 (Fe)[1] due to the evaporation of these guests during the PXRD measurements.

Supplementary references

1 Millange, F., Serre, C., Guillou, N., Férey, G. & Walton, R. I. Structural effects of solvents on the breathing of metal-organic frameworks: an in situ diffraction study. *Angew. Chem. Int. Ed. Engl.* **47**, 4100-4105 (2008). https://doi.org:10.1002/anie.200705607

2 Sun, L. *et al.* Room-Temperature Quantitative Quantum Sensing of Lithium Ions with a Radical-Embedded Metal-Organic Framework. *J. Am. Chem. Soc.* **144**, 19008-19016 (2022). https://doi.org:10.1021/jacs.2c07692

3 Yamauchi, S. *et al.* The Lowest Photoexcited Triplet State of Subphthalocyanine in Solid and Fluid Environments. Time-Resolved Electron Paramagnetic Resonance Studies. *J. Phys. Chem. A* **107**, 1478-1485 (2003). https://doi.org:10.1021/jp0258210

4 Loiseau, T. *et al.* A rationale for the large breathing of the porous aluminum terephthalate (MIL-53) upon hydration. *Chem. Eur. J.* **10**, 1373-1382 (2004). https://doi.org:10.1002/chem.200305413

5 Fujiwara, S. *et al.* Triplet Dynamic Nuclear Polarization of Guest Molecules through Induced Fit in a Flexible Metal–Organic Framework. *Angew. Chem. Int. Ed. Engl.* **61**, e202115792 (2022). https://doi.org:10.1002/anie.202115792